Time-Domain Three-Dimensional Diffraction by the Isorefractive Wedge

Robert W. Scharstein and Anthony M. J. Davis

***Abstract*—The extension of the Biot–Tolstoy exact time domain solution to the electromagnetic isovelocity or isorefractive wedge is described. The TM field generated by a Hertzian electric dipole can be represented by a vector potential parallel to the apex of the wedge and a scalar potential necessitated by the three dimensionality of the magnetic field. The derivation of the former is exactly that of the pressure in the corresponding acoustic situation [1], and a more efficient version of the lengthy details is presented herein. A Lorentz gauge determines the scalar potential from the vector potential, and the diffracted field contains impulsive and "switch-on" terms that cannot be evaluated in closed form. The ratio of arrival times, at a given point, of the geometrical optics and diffracted fields provides a convenient parameter, in addition to the usual metric-related variable, for graphically displaying this scalar potential.**

***Index Terms*— Boundary value problems, electromagnetic diffraction, electromagnetic scattering, transforms, transient analysis, wedge.**

I. Introduction

THE RECENT solution [1] for the acoustic wave scattered by the isovelocity wedge is adapted to the electromagnetic case. In [1], a succession of integral transforms is applied to the pertinent transmission problem for the three-dimensional time domain wave equation in the spirit of the Biot–Tolstoy solution [2] of the simpler impenetrable wedge. The Biot–Tolstoy exact solution to the canonical soft/hard wedge diffraction is often cited in the acoustics literature and is the basic building block of a time domain analog of geometrical theory of diffraction (GTD) modeling called the "wedge assemblage method" [3]. The application of the Biot and Tolstoy ideas to the TM/TE electromagnetic scattering by the perfectly conducting wedge was presented by Felsen [4] and is mentioned in the Soviet translation [5]. However, our electromagnetics community has apparently ignored this interesting time domain solution in favor of, for example, numerical Fourier transformation of the time-harmonic GTD results [6]. Analytic Fourier transformation of the GTD (UTD) diffraction for a curved wedge is applied in [7] to exciting pulses that have appropriate high-pass and band-pass spectra.

Henceforth, the present paper extends the time domain analysis to the electromagnetic scattering by a penetrable, albeit isovelocity, wedge. The perfectly conducting wedge can be recovered as a special case. As indicated in [1] and recognized by [8] and [9], the main value of the isovelocity solution is its service, in principle, as the zeroth-order iterate for a wedge of relatively small velocity contrast. However, the envisaged perturbative adjustment (i.e., Neumann series) cannot be constructed in the time domain because an upper bound must be imposed on the frequency. A complete or even usable solution for the arbitrary penetrable (i.e., dielectric) wedge is not yet available. Marx [10] and Davis [11] give complementary views of the status of the two-dimensional frequency domain version of this problem for which Rawlins [12] gave a one-term perturbation for the right-angled wedge with equal density.

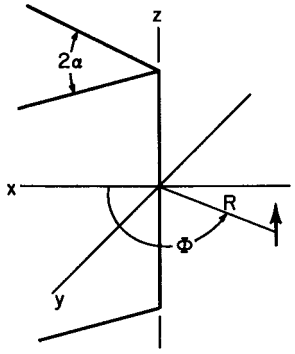

Fig. 1. Wedge and Hertzian dipole.

The source is an impulsive Hertzian dipole, situated at the point with cylindrical coordinates $(R, \Phi, 0)$, in the exterior region and oriented parallel to the edge of the wedge, i.e., in the $\hat{z}$ direction (Fig. 1). The constitutive parameters of the lossless external (e) and internal (i) media satisfy the requirement that the intrinsic wave speed remains invariant

$$c = (\mu_e \epsilon_e)^{-1/2} = (\mu_i \epsilon_i)^{-1/2}. \tag{1}$$

The name "diaphanous" refers to similar wave speeds in [13], but is adopted by [8] for this isovelocity or isorefractive wedge, with intrinsic impedance $\sqrt{\mu_i/\epsilon_i}$, which clearly differs, in general, from the external impedance $\sqrt{\mu_e/\epsilon_e}$. This is exactly analogous to the archetypal scattering problem of the density contrast wedge [1].

Axially directed electric and magnetic dipoles are considered because of the concomitant simplification in describing vector fields that are TM $(H_z \equiv 0)$ and TE $(E_z \equiv 0)$, respectively. Further rationalization for avoiding generally oriented dipoles appeals to the TM/TE decomposition of arbitrary electromagnetic fields, external to the source. Spherical

Manuscript received June 2, 1997; revised December 8, 1997.

R. W. Scharstein is with the Electrical Engineering Department, University of Alabama, Tuscaloosa, AL 35487 USA.

A. M. J. Davis is with the Mathematics Department, University of Alabama, Tuscaloosa, AL 35487 USA.

Publisher Item Identifier S 0018-926X(98)06097-9.

coordinates (s, θ, ϕ) and (S, Θ, Φ) can be introduced, if desired, via

$$\begin{aligned} R &= S\sin\Theta \qquad r = s\sin\theta \\ Z &= S\cos\Theta \qquad z = s\cos\theta \end{aligned} \tag{2}$$

where $(z - Z)$ replaces z as the axial displacement between the field and source points. As the radial distance to the source $S \to \infty$, the incident wavefront becomes planar. Similarly, the far scattered field is measured by distant observers at large s. The steady-state behavior of monochromatic fields permits a natural distinction between "near" and "far" fields according to a radial scale that depends upon the wavelength and source dimension. In contrast, the temporal evolution of the Dirac delta singularities and subsequent derivatives in this time domain solution obscure the demarcation between near and far fields. Therefore, it is important to examine the structure of the entire field.

The geometry of Fig. 1 suggests that the field behavior at any point is appropriately represented as a function of the four coordinates (r, ϕ, z, t). In the diffraction analysis of [1], the time and length coordinates become combined with the wave speed c in the metric-related variable ξ, defined by

$$\cosh\xi = \frac{(ct)^2 - (R^2 + r^2 + z^2)}{2Rr} \geq 1. \tag{3}$$

In [1], the underlying scalar boundary value problem is solved, and explicit solutions for the subject wave function are presented for several cases of wedge angle, notably $\alpha = \pi/4$, $\pi/3$, $2\pi/5$, and $\pi/6$. The physics of the present electromagnetic problem are conveniently represented in terms of two functions—the vector and scalar potentials. After the statement of the potential wave equations and transmission conditions at the wedge boundary in Section II, the philosophy and details of the integral transform analysis are summarized in Section III. An efficient summation of resultant residue series is presented in Section IV for the case of wedge angles that are rational multiples of π. Calculations of the geometrical optics and diffraction field are detailed in Appendixes A and B, respectively, for specific wedges of half angle $\alpha = \pi/3$ and $\pi/4$. Calculated results for the time/space behavior of the electromagnetic potentials are graphed for some selected physical parameters for the case $\alpha = \pi/4$ in Section V. As in the standard time-harmonic scattering from the perfectly conducting wedge, the most interesting feature of this full electrodynamic solution is the singular behavior of the diffracted field at the critical reflection and shadow boundaries of the geometrical optics field. Otherwise, the general nature of the waveforms, except for straightforward scale factors, is reasonably insensitive to the particular wedge angle and to the degree of impedance contrast.

II. Boundary Value Problem for the Potentials

A. Hertzian Electric Dipole

All fields are functions of space and time in the manner of $\vec{E}(\vec{r}, t) = \vec{E}(r, \phi, z, t)$. The Hertzian electric dipole of Fig. 1 is represented by the volume density of electric current

$$\vec{J}(r, \phi, z, t) = \hat{z} I\ell \frac{\delta(r - R)}{R}\,\delta(\phi - \Phi)\delta(z)\delta(t). \tag{4}$$

Continuity of charge requires the accompanying volume density of electric charge

$$\rho_v(r, \phi, z, t) = -I\ell \frac{\delta(r - R)}{R}\,\delta(\phi - \Phi)\delta'(z)H(t) \tag{5}$$

which is an electrostatic dipole created by the impulsive current at time $t = 0$. Symmetry about the wedge bisector allows the source angle to be restricted to the range $\alpha < \Phi < \pi$. A vector magnetic potential $\vec{A}$ and a scalar electric potential V, defined by

$$\vec{H} = \epsilon \nabla \times \vec{A}$$

and

$$\vec{E} = -\nabla V - \frac{1}{c^2}\frac{\partial \vec{A}}{\partial t} \tag{6}$$

are introduced into the Maxwell equations, subject to a Lorentz gauge $\nabla \cdot \vec{A} = -\partial V/\partial t$. This scaling is chosen to allow the direct comparison with the boundary conditions in [1].

The particular solution for the vector potential in the cylindrical coordinate system of Fig. 1 is $\vec{A}(\vec{r}, t) = \hat{z} A_z(\vec{r}, t)$. Consider a smooth closed contour C in the (x, y) plane, with outward normal $\hat{n}$ and tangent unit vector $\hat{\tau} = \hat{z} \times \hat{n}$. On the boundary C, the tangential component of the magnetic field intensity is proportional to

$$\hat{n} \times \vec{H} = -\hat{z}\epsilon \frac{\partial A_z}{\partial n}. \tag{7}$$

The boundary condition of continuity of tangential $\vec{H}$ therefore requires continuity of $\epsilon \partial A_z/\partial n$ along the curve that separates the two homogeneous regions. Similarly, away from the source, $\partial \vec{E}/\partial t = \nabla \times \nabla \times \vec{A}$ implies

$$\hat{n} \times \frac{\partial \vec{E}}{\partial t} = \hat{\tau}\left[\frac{\partial^2 A_z}{\partial \tau^2} + \frac{\partial^2 A_z}{\partial n^2}\right] + \hat{z}\,\frac{\partial^2 A_z}{\partial z\,\partial \tau} \tag{8}$$

and thus continuity of tangential $\vec{E}$ translates, for all time, to continuity of the vector potential A_z at each point of the boundary. With $\vec{A}$ properly specified, the boundary condition on tangential $\vec{E}$ now implies continuity of V and the absence of free surface charge requires continuity of $\epsilon \partial V/\partial n$.

The scalar boundary value problems for both potential functions in the exterior and interior wedge regions consist of inhomogeneous wave equations

$$\begin{aligned} &\left(\nabla^2 - \frac{1}{c^2}\frac{\partial^2}{\partial t^2}\right)\begin{Bmatrix} A_z^{(e)}(r, \phi, z, t) \\ V^{(e)}(r, \phi, z, t) \end{Bmatrix} \\ &\quad = \mp\frac{I\ell}{\epsilon_e}\frac{\delta(r - R)}{R}\,\delta(\phi - \Phi)\begin{Bmatrix} \delta(z)\delta(t) \\ \delta'(z)H(t) \end{Bmatrix} \\ &\qquad (\alpha < \Phi < \pi,\ \alpha < \phi < 2\pi - \alpha) \\ &\left(\nabla^2 - \frac{1}{c^2}\frac{\partial^2}{\partial t^2}\right)\begin{Bmatrix} A_z^{(i)}(r, \phi, z, t) \\ V^{(i)}(r, \phi, z, t) \end{Bmatrix} \\ &\quad = 0 \qquad (-\alpha < \phi < \alpha) \end{aligned} \tag{9}$$

subject to identical boundary conditions

$$\left\{\begin{matrix} A_z^{(e)} = A_z^{(i)} \\ V^{(e)} = V^{(i)} \end{matrix}\right\} \quad \text{and} \quad \left\{\begin{matrix} \rho \dfrac{\partial A_z^{(e)}}{\partial \phi} = \dfrac{\partial A_z^{(i)}}{\partial \phi} \\ \rho \dfrac{\partial V^{(e)}}{\partial \phi} = \dfrac{\partial V^{(i)}}{\partial \phi} \end{matrix}\right\} \text{ at } \phi = \pm\alpha \tag{10}$$

where the permittivity ratio is $\rho = \epsilon_e/\epsilon_i$. In this case of electric dipole source, which is the TM or E polarization, it is expedient to define the reflection coefficient

$$\Gamma = \frac{\rho - 1}{\rho + 1} = \frac{\epsilon_e - \epsilon_i}{\epsilon_e + \epsilon_i}. \tag{11}$$

The perfectly conducting wedge is the limiting case $\Gamma = -1$. Note that the two solutions A_z and V are related, as are their respective forcing functions in (9), by the Lorentz gauge

$$V(r, \phi, z, t) = -\int_{-\infty}^{t} \frac{\partial}{\partial z} A_z(r, \phi, z, t')\, dt' \tag{12}$$

consistent with the introduction of V being necessitated by the dependence of $\vec{H}$ on z.

B. Hertzian Magnetic Dipole

TE or H polarization is the perfect dual of the preceding case. Therefore, the above analysis applies to the magnetic dipole, after making the following substitutions. Exchange magnetic dipole moment $K\ell$ for the electric dipole moment $I\ell$ of the source, and write $\vec{E} = -\mu\nabla\times\vec{F}$ in terms of a $\hat{z}$ directed vector electric potential. That is, make the dual replacements

$$\begin{aligned} &A_z \Rightarrow F_z \quad V \Rightarrow U \quad \epsilon \Rightarrow \mu \quad \mu \Rightarrow \epsilon \\ &\vec{H} \Rightarrow -\vec{E} \quad \vec{E} \Rightarrow \vec{H}. \end{aligned} \tag{13}$$

In particular, the pair of scalar functions F_z and U satisfies the same partial differential equations (9) and transmission conditions (10), where ρ is now the permeability ratio μ_e/μ_i. The magnetic reflection coefficient is thus

$$\Gamma_m = \frac{\mu_e - \mu_i}{\mu_e + \mu_i} \tag{14}$$

which is $-\Gamma$ of the dual problem, according to the isovelocity condition (1). In light of this direct duality, only the TM or E polarization is considered in the remainder of this work.

III. Transform Analysis for the Isorefractive Wedge

A suitable scaling of the forcing term permits the electromagnetic equations of (9) and (10) for the vector potential to be rewritten precisely in the acoustics notation of [1]:

$$\begin{aligned} &\left(\nabla^2 - \frac{1}{c^2}\frac{\partial^2}{\partial t^2}\right) p^{(e)}(r, \phi, z, t) \\ &\quad = \frac{\delta(r - R)}{R}\delta(\phi - \Phi)\delta(z)\delta(t) \\ &\qquad (\alpha < \Phi < \pi,\ \alpha < \phi < 2\pi - \alpha) \\ &\left(\nabla^2 - \frac{1}{c^2}\frac{\partial^2}{\partial t^2}\right) p^{(i)}(r, \phi, z, t) \\ &\quad = 0 \qquad (-\alpha < \phi < \alpha) \end{aligned} \tag{15}$$

subject to the boundary conditions

$$p^{(e)} = p^{(i)} \quad \text{and} \quad \rho\frac{\partial p^{(e)}}{\partial \phi} = \frac{\partial p^{(i)}}{\partial \phi} \quad \text{at } \phi = \pm\alpha. \tag{16}$$

This boundary value problem can be solved by introducing a Fourier transform in both t and z according to

$$\hat{p}(r, \phi, \ell, \omega) = 2\int_{-\infty}^{\infty} e^{-i\omega t}\int_{0}^{\infty} p(r, \phi, z, t)\cos \ell z\, dz\, dt \tag{17}$$

with the definitions $k = \omega/c$, $\kappa = \sqrt{k^2 - \ell^2}$, followed by a Kantorovich–Lebedev transform in the radial coordinate. This yields

$$\begin{aligned} \hat{p}(r, \phi, \kappa) = \lim_{\epsilon\to 0} -\tfrac{1}{4}\int_{-i\infty}^{i\infty} &\exp(\epsilon\nu^2) J_\nu(\kappa r) \\ &\cdot H_\nu^{(2)}(\kappa R) f(\nu, \phi)\, d\nu \end{aligned} \tag{18}$$

which, by adapting [13, (9.19)], can be rearranged as

$$\begin{aligned} \hat{p}(r, \phi, \kappa) = \tfrac{1}{4}\int_{\infty-\pi i}^{\infty+\pi i} &H_0^{(2)}[\kappa(r^2 + R^2 - 2rR\cosh w)^{1/2}] \\ &\cdot \sum_{m=0}^{\infty}{}'[\operatorname{res}\{e^{-\nu w} f(\nu, \phi)\} \text{ at } \nu = \nu_m]\, dw \end{aligned} \tag{19}$$

where res{ } denotes a residue and for the external region

$$\begin{aligned} f &= f^{(e)} \\ &= \frac{\cos\nu\Phi + \Gamma\cos\nu(\Phi - 2\alpha)}{\sin\nu\pi + \Gamma\sin\nu(\pi - 2\alpha)}\cos\nu(\pi - \phi) \\ &\quad \pm \frac{-\sin\nu\Phi + \Gamma\sin\nu(\Phi - 2\alpha)}{\sin\nu\pi - \Gamma\sin\nu(\pi - 2\alpha)}\sin\nu(\pi - \phi) \\ &\quad + (1 \pm 1)H(\Phi - \phi)\sin\nu(\Phi - \phi) \\ &\qquad (\alpha < \phi < \pi) \end{aligned} \tag{20}$$

according as the source is at $(R, \Phi, 0)$ or $(R, 2\pi - \Phi, 0)$. Here, $|\Gamma| \le 1$, the w integration above is along the contour that passes to the left of the point $w = \cosh^{-1}[r^2 + R^2 + z^2)/2rR]$, the poles are indexed $\nu_0 = 0$, $\nu_m > \nu_{m-1}$ $(m \ge 1)$, and the prime on the summation denotes that a 1/2 factor multiplies the residue at the origin, if it exists. Inversion of the z and t transforms yields

$$\begin{aligned} &p(r, \phi, z, t) \\ &\quad = \frac{i}{4\pi}\int_{\infty-\pi i}^{\infty+\pi i} \frac{\delta\left[t - \dfrac{1}{c}(r^2 + R^2 - 2rR\cosh w + z^2)^{1/2}\right]}{(r^2 + R^2 - 2rR\cosh w + z^2)^{1/2}} \\ &\qquad \cdot \sum_{m=0}^{\infty}{}'[\operatorname{res}\{e^{-\nu w} f(\nu, \phi)\} \text{ at } \nu = \nu_m]\, dw \end{aligned} \tag{21}$$

and subsequent deformation of the contour shows that

$$\begin{aligned} p(r, \phi, z, t) = -\frac{1}{2\pi}\frac{c}{rR\sin\eta}&\sum_{m=0}^{\infty}{}' \\ &\cdot [\operatorname{res}\{\cos\nu\eta\, f(\nu, \phi)\} \text{ at } \nu = \nu_m] \\ &+ \frac{1}{2\pi}\frac{c}{rR\sinh\xi}\sum_{m=1}^{\infty} \\ &\cdot [\operatorname{res}\{e^{-\nu\xi}\sin\nu\pi\, f(\nu, \phi)\} \text{ at } \nu = \nu_m] \end{aligned} \tag{22}$$

where the time and space dependence is folded into

$$\cos\eta = \frac{R^2+r^2+z^2-c^2t^2}{2Rr} \qquad \left(\sqrt{(R-r)^2+z^2} < ct < \sqrt{(R+r)^2+z^2}\right)$$
$$\cosh\xi = \frac{c^2t^2-R^2-r^2-z^2}{2Rr} \qquad \left(ct > \sqrt{(R+r)^2+z^2}\right) \tag{23}$$

with $0 < \eta < \pi$ and contributions occurring in relevant time intervals.

Thus, the evaluation of the field involves the summation of these residue series. In the soft and hard cases (TM and TE polarization, respectively, for the perfectly conducting wedge), the poles are integers or half integers and the summations are elementary. These are the Biot–Tolstoy solutions [2] that were rederived by Felsen [4], and further details are given in [1] in the verification of this limiting case of no penetration. In general, the poles are the roots of transcendental equations and the corresponding residues appear to defy summation. However, some simplification occurs if the wedge angle is a rational multiple of π, since then the residue series reduce to a finite number of summable series. Even these are nontrivial since the roots of polynomials must be determined and so the presented results are necessarily restricted to rational multiples involving small integers.

IV. Wedge Angle: A Rational Multiple of π

After setting

$$\frac{\pi-2\alpha}{\pi} = \frac{N}{M} \tag{24}$$

the combinations M, N, both odd and M or N even, were considered separately in [1], but here the presentation is suitably modified so that this distinction is unnecessary. The consequent simplification is readily apparent, e.g., only the $\{y_i\}$ roots are used.

With the definition

$$F_{\pm}^{(e)}(\nu) = \frac{1}{4}\,\frac{\cos\nu\pi \pm \Gamma\cos\nu(\pi-2\alpha)}{\sin\nu\pi \pm \Gamma\sin\nu(\pi-2\alpha)} \tag{25}$$

the symmetric and antisymmetric versions of (20) are

$$\begin{aligned} f_{s,a}^{(e)} &= 4F_{\pm}^{(e)}(\nu)\begin{matrix}\cos\\ \sin\end{matrix}\nu(\pi-\Phi)\begin{matrix}\cos\\ \sin\end{matrix}\nu(\pi-\phi) \\ &\quad + \text{regular function} \\ &= 2F_{\pm}^{(e)}(\nu)[\cos\nu(\Phi-\phi) \pm \cos\nu(2\pi-\Phi-\phi)] \\ &\quad + \text{regular function} \end{aligned} \tag{26}$$

so that

$$\begin{aligned} &\operatorname{res}\{\cos\nu\eta[f_s^{(e)}(\nu,\phi) \pm f_a^{(e)}(\nu,\phi)]\} \\ &\quad = \operatorname{res}\{[F_+^{(e)}(\nu) \pm F_-^{(e)}(\nu)][\cos\nu(\eta+|\Phi-\phi|) \\ &\qquad + \cos\nu(\eta-|\Phi-\phi|)]\} \\ &\qquad + \operatorname{res}\{[F_+^{(e)}(\nu) \mp F_-^{(e)}(\nu)][\cos\nu(\eta+2\pi-\Phi-\phi) \\ &\qquad\quad + \cos\nu(\eta-2\pi+\Phi+\phi|)]\} \end{aligned} \tag{27}$$

which is required for $p_s \pm p_a$. Thus we need to consider, for various choices of Ω, the series

$$\sum_{m=0}^{\infty}{}'[\operatorname{res}\{[F_+^{(e)}(\nu) \pm F_-^{(e)}(\nu)]\cos\nu\Omega\} \text{ at } \nu=\nu_m]. \tag{28}$$

With $\theta = \nu\pi/M$, $x = \cos\theta$, as in [1], (25) is expressed as

$$F_{\pm}^{(e)}(\nu) = \frac{1}{4\sin\theta}\,\frac{T_M(x) \pm \Gamma T_N(x)}{U_{M-1}(x) \pm \Gamma U_{N-1}(x)} \tag{29}$$

in terms of Chebyshev polynomials

$$\begin{aligned} T_N(x) &= \cos N\theta \\ U_N(x) &= \frac{\sin(N+1)\theta}{\sin\theta} \qquad (N \geq 0). \end{aligned} \tag{30}$$

The residue of $F_{\pm}^{(e)}(\nu)$ at $\theta = k\pi$, i.e., at $\nu = kM$ $(k \geq 0)$ is, from (29) and (30)

$$\frac{M}{4\pi}\,\frac{(-1)^{kM} \pm \Gamma(-1)^{kN}}{M(-1)^{kM} \pm \Gamma N(-1)^{kN}} \tag{31}$$

and, hence, the required sum/difference in (28) is

$$\begin{aligned} &\frac{M}{4\pi}\left[\frac{(-1)^{k(M-N)}+\Gamma}{M(-1)^{k(N-M)}+\Gamma N} \pm \frac{(-1)^{k(M-N)}-\Gamma}{M(-1)^{k(N-M)}-\Gamma N}\right] \\ &\quad = \frac{M}{2\pi(M^2-\Gamma^2N^2)}\begin{Bmatrix} M-\Gamma^2N \\ \Gamma(-1)^{k(N-M)}(M-N)\end{Bmatrix}. \end{aligned} \tag{32}$$

The generalized Fourier series

$$\begin{aligned} \sum_{k=0}^{\infty}{}'\cos kM\Omega &= \tfrac{1}{2}\sum_{k=-\infty}^{\infty} e^{ikM\Omega} \\ &= \pi\mathring{\delta}(M\Omega) \\ &= \pi\sum_{n=-\infty}^{\infty}\delta(M\Omega-2n\pi) \\ &= \frac{\pi}{M}\sum_{n=-\infty}^{\infty}\delta(\Omega-2n\pi/M) \end{aligned} \tag{33}$$

and

$$\begin{aligned} \sum_{k=0}^{\infty}{}'(-1)^{kL}\cos kM\Omega &= \sum_{k=0}^{\infty}{}'\cos k(M\Omega+L\pi) \\ &= \frac{\pi}{M}\sum_{n=-\infty}^{\infty}\delta[\Omega-(2n-L)\pi/M] \end{aligned} \tag{34}$$

allow the reductions

$$\begin{aligned} &\sum_{k=0}^{\infty}{}'[\operatorname{res}\{[F_+^{(e)}(\nu)+F_-^{(e)}(\nu)]\cos\nu\Omega\} \text{ at } \nu=kM] \\ &\quad = \frac{M-\Gamma^2N}{2(M^2-\Gamma^2N^2)}\sum_{n=-\infty}^{\infty}\delta(\Omega-2n\pi/M) \end{aligned} \tag{35}$$

and

$$\sum_{k=0}^{\infty}{}'[\text{res}\{[F_+^{(e)}(\nu)-F_-^{(e)}(\nu)]\cos\nu\Omega\}\text{ at }\nu=kM] = \frac{\Gamma(M-N)}{2(M^2-\Gamma^2N^2)}\sum_{n=-\infty}^{\infty}\delta[\Omega-(2n-M+N)\pi/M]. \tag{36}$$

The Dirac-delta functions, arising from the first residue sum of (22), are the geometrical optics portion of the total field, while the second series in (22) is the diffraction field.

Further consideration of the sum and difference of (25) proceeds with the form

$$F_+^{(e)}(\nu)\pm F_-^{(e)}(\nu) = \frac{1}{4}\left[\frac{\cos M\theta+\Gamma\cos N\theta}{\sin M\theta+\Gamma\sin N\theta}\pm\frac{\cos M\theta-\Gamma\cos N\theta}{\sin M\theta-\Gamma\sin N\theta}\right] = \frac{1}{4(\sin^2 M\theta-\Gamma^2\sin^2 N\theta)}\begin{Bmatrix}\sin 2M\theta-\Gamma^2\sin 2N\theta\\ 2\Gamma\sin(M-N)\theta\end{Bmatrix}. \tag{37}$$

Pairs of residues differ by only a ±1 factor according as to whether the pole arises at a zero of $\sin M\theta\pm\Gamma\sin N\theta$. Let $y=\cos 2\theta=\cos(2\nu\pi/M)$; then the poles of (37) occur at the zeros of $1-\Gamma^2-T_M(y)+\Gamma^2T_N(y)$, i.e., at $y_1, y_2, \cdots, y_{M-1}$, 1. The zero at $y=1$ corresponds to the already considered poles at $\nu=kM$. The other roots correspond to

$$\nu=kM\pm\frac{M}{2\pi}\cos^{-1}y_i\qquad\left(k\geq\begin{matrix}0\\1\end{matrix}\right). \tag{38}$$

The residue of $F_+^{(e)}(\nu)+F_-^{(e)}(\nu)$ at $\nu=kM\pm(M/2\pi)\cos^{-1}y_i$ is, from (37)

$$\frac{M}{4\pi}\frac{\sin 2M\theta-\Gamma^2\sin 2N\theta}{M\sin 2M\theta-\Gamma^2N\sin 2N\theta}\bigg|_{2\theta=2k\pi\pm\cos^{-1}y_i} = \frac{M}{4\pi}\frac{U_{M-1}(y_i)-\Gamma^2U_{N-1}(y_i)}{MU_{M-1}(y_i)-\Gamma^2NU_{N-1}(y_i)} \tag{39}$$

and furthermore

$$\sum_{k=0}^{\infty}{}'\left[\text{res}\{[F_+^{(e)}(\nu)+F_-^{(e)}(\nu)]\cos\nu\Omega\}\text{ at }\nu=kM\pm\frac{M}{2\pi}\cos^{-1}y_i\right]\qquad\left(k\geq\begin{matrix}0\\1\end{matrix}\right) = \frac{M}{2\pi}\frac{U_{M-1}(y_i)-\Gamma^2U_{N-1}(y_i)}{MU_{M-1}(y_i)-\Gamma^2NU_{N-1}(y_i)}\cdot\sum_{k=0}^{\infty}{}'\cos kM\Omega\cos\left[\frac{M\Omega}{2\pi}\cos^{-1}y_i\right] = \frac{1}{2}\frac{U_{M-1}(y_i)-\Gamma^2U_{N-1}(y_i)}{MU_{M-1}(y_i)-\Gamma^2NU_{N-1}(y_i)}\cdot\sum_{n=-\infty}^{\infty}\delta(\Omega-2n\pi/M)T_{|n|}(y_i). \tag{40}$$

Similarly, the residue of $F_+^{(e)}(\nu)-F_-^{(e)}(\nu)$ at $\nu=kM\pm(M/2\pi)\cos^{-1}y_i$ is

$$\frac{M\Gamma}{2\pi}\frac{\sin(M-N)\theta}{M\sin 2M\theta-\Gamma^2N\sin 2N\theta}\bigg|_{2\theta=2k\pi\pm\cos^{-1}y_i} = \frac{M\Gamma}{2\pi}\frac{(-1)^{(M-N)k}\sin\left[\frac{M-N}{2}\cos^{-1}y_i\right]}{[MU_{M-1}(y_i)-\Gamma^2NU_{N-1}(y_i)]\sin(\cos^{-1}y_i)} \tag{41}$$

which is needed in

$$\sum_{k=0}^{\infty}{}'\left[\text{res}\{[F_+^{(e)}(\nu)-F_-^{(e)}(\nu)]\cos\nu\Omega\}\text{ at }\nu=kM\pm\frac{M}{2\pi}\cos^{-1}y_i\right]\qquad\left(k\geq\begin{matrix}0\\1\end{matrix}\right) = \frac{M\Gamma}{\pi}\frac{\sin\left[\frac{M-N}{2}\cos^{-1}y_i\right]}{[U_{M-1}(y_i)-\Gamma^2NU_{N-1}(y_i)]\sin(\cos^{-1}y_i)}\cdot\sum_{k=0}^{\infty}{}'(-1)^{k(M-N)}\cos kM\Omega\cos\left[\frac{M\Omega}{2\pi}\cos^{-1}y_i\right] = \frac{\Gamma\sin\left[\frac{M-N}{2}\cos^{-1}y_i\right]}{[MU_{M-1}(y_i)-\Gamma^2NU_{N-1}(y_i)]\sin(\cos^{-1}y_i)}\cdot\sum_{n=-\infty}^{\infty}\delta\left[\Omega-\frac{2n-M+N}{M}\pi\right]\cdot\cos\left[\left(n-\frac{M-N}{2}\right)\cos^{-1}y_i\right] = \frac{\Gamma}{2[MU_{M-1}(y_i)-\Gamma^2NU_{N-1}(y_i)]}\cdot\sum_{n=-\infty}^{\infty}\delta[\Omega-(2n-M+N)\pi/M]\cdot\{\text{sgn}\,n\,U_{|n|-1}(y_i)-\text{sgn}(n-M+N)\cdot U_{|n-M+N|-1}(y_i)\}. \tag{42}$$

Thus, by combining (35) and (40)

$$\sum_{m=0}^{\infty}{}'[\text{res}\{[F_+^{(e)}(\nu)+F_-^{(e)}(\nu)]\cos\nu\Omega\}\text{ at }\nu=\nu_m] = \sum_{n=-\infty}^{\infty}\delta(\Omega-2n\pi/M)\left\{\frac{M-\Gamma^2N}{2(M^2-\Gamma^2N^2)}+\frac{1}{2}\sum_{i=1}^{M-1}\frac{U_{M-1}(y_i)-\Gamma^2U_{N-1}(y_i)}{MU_{M-1}(y_i)-\Gamma^2NU_{N-1}(y_i)}T_{|n|}(y_i)\right\}. \tag{43}$$

Similarly, from (36) and (42), the difference sum is shown in (44) at the bottom of the next page. When $M-N$ is even, the second summation can be expressed in terms of $\delta(\Omega-2n\pi/M)$ by replacing n by $n+(M-N)/2$ in (44), whereupon the

expression in { } reduces to

$$\frac{\Gamma(M-N)}{2(M^2-\Gamma^2N^2)}+\Gamma\sum_{i=1}^{M-1}\frac{U_{((M-N)/2)-1}(y_i)T_{|n|}(y_i)}{MU_{M-1}(y_i)-\Gamma^2NU_{N-1}(y_i)}. \tag{45}$$

The diffracted terms in the second sum of (22) are now written in the form

$$\begin{aligned}&\operatorname{res}\{e^{-\nu\xi}\sin\nu\pi[f_s^{(e)}(\nu,\phi)\pm f_a^{(e)}(\nu,\phi)]\}\\&\quad=\operatorname{res}\{[F_+^{(e)}(\nu)\pm F_-^{(e)}(\nu)]e^{-\nu\xi}\sin\nu\pi\\&\qquad\cdot 2\cos\nu(\Phi-\phi)\}\\&\qquad+\operatorname{res}\{[F_+^{(e)}(\nu)\mp F_-^{(e)}(\nu)]e^{-\nu\xi}\sin\nu\pi\\&\qquad\cdot 2\cos\nu(2\pi-\Phi-\phi)\}\end{aligned} \tag{46}$$

which is required for $p_s\pm p_a$. The general form of the residue sums is therefore

$$\sum_{m=1}^{\infty}[\operatorname{res}\{[F_+^{(e)}(\nu)\pm F_-^{(e)}(\nu)]e^{-\nu\xi}\sin\nu\pi\cdot 2\cos\nu\Psi\}\ \text{at}\ \nu=\nu_m]. \tag{47}$$

There are no poles at $\nu=kM$, and, hence, the contributions of the poles (38) to the residue sum (47) with the plus sign are by using (42)

$$\begin{aligned}&\frac{M}{2\pi}\frac{U_{M-1}(y_i)-\Gamma^2U_{N-1}(y_i)}{MU_{M-1}(y_i)-\Gamma^2NU_{N-1}(y_i)}\sin\left(\frac{M}{2}\cos^{-1}y_i\right)\\&\quad\cdot\Re\left\{\exp\left[-(\xi-i\Psi)\frac{M}{2\pi}\cos^{-1}y_i\right]\right.\\&\qquad\cdot\sum_{k=0}^{\infty}(-1)^{kM}e^{-kM(\xi-i\Psi)}\\&\qquad-\exp\left[(\xi-i\Psi)\frac{M}{2\pi}\cos^{-1}y_i\right]\\&\qquad\left.\cdot\sum_{k=1}^{\infty}(-1)^{kM}e^{-kM(\xi-i\Psi)}\right\}\end{aligned} \tag{48}$$

in which, by summing the geometric series, the complex factor reduces to as shown in (49), given at the bottom of the next page. The first desired residue sum in (47) is therefore, by substituting (48) and (49)

$$\begin{aligned}&\sum_{m=1}^{\infty}[\operatorname{res}\{[F_+^{(e)}(\nu)+F_-^{(e)}(\nu)]e^{-\nu\xi}\sin\nu\pi\cdot 2\cos\nu\Psi\}\\&\qquad\text{at}\ \nu=\nu_m]\\&=\frac{M}{2\pi}\sum_{i=1}^{M-1}\frac{U_{M-1}(y_i)-\Gamma^2U_{N-1}(y_i)}{MU_{M-1}(y_i)-\Gamma^2NU_{N-1}(y_i)}\\&\quad\cdot\frac{\sin\left(\frac{M}{2}\cos^{-1}y_i\right)}{\cosh M\xi-(-1)^M\cos M\Psi}\\&\quad\cdot\left\{\cosh\left[M\xi\left(1-\frac{1}{2\pi}\cos^{-1}y_i\right)\right]\right.\\&\quad\cdot\cos\left[\frac{M\Psi}{2\pi}\cos^{-1}y_i\right]-(-1)^M\cosh\left[\frac{M\xi}{2\pi}\cos^{-1}y_i\right]\\&\quad\left.\cdot\cos\left[M\Psi\left(1-\frac{1}{2\pi}\cos^{-1}y_i\right)\right]\right\}\end{aligned} \tag{50}$$

and similarly, by using (41)

$$\begin{aligned}&\sum_{m=1}^{\infty}[\operatorname{res}\{[F_+^{(e)}(\nu)-F_-^{(e)}(\nu)]e^{-\nu\xi}\sin\nu\pi\cdot 2\cos\nu\Psi\}\\&\qquad\text{at}\ \nu=\nu_m]\\&=\frac{M\Gamma}{\pi}\sum_{i=1}^{M-1}\frac{\sin\left[\frac{M-N}{2}\cos^{-1}y_i\right]}{[MU_{M-1}(y_i)-\Gamma^2NU_{N-1}(y_i)]\sin(\cos^{-1}y_i)}\\&\quad\cdot\frac{\sin\left(\frac{M}{2}\cos^{-1}y_i\right)}{\cosh M\xi-(-1)^N\cos M\Psi}\\&\quad\cdot\left\{\cosh\left[M\xi\left(1-\frac{1}{2\pi}\cos^{-1}y_i\right)\right]\cos\left[\frac{M\Psi}{2\pi}\cos^{-1}y_i\right]\right.\\&\qquad-(-1)^N\cosh\left[\frac{M\xi}{2\pi}\cos^{-1}y_i\right]\\&\qquad\left.\cdot\cos\left[M\Psi\left(1-\frac{1}{2\pi}\cos^{-1}y_i\right)\right]\right\}.\end{aligned} \tag{51}$$

For p_s+p_a, take the first sum with $\Psi=|\Phi-\phi|$ and the second sum with $\Psi=2\pi-\Phi-\phi$ and sum over i. For the difference p_s-p_a, do likewise with the angles interchanged.

V. Application to the Right-Angled Wedge

When $\alpha=\pi/4$, the complete solution of (9) and (10) for the vector potential in the exterior region is assembled from the sample results in Appendixes A and B. As indicated above, an alternate calculation of the relevant residue sums is given in [1]. If the field point is on the same side of the symmetry plane as the source, i.e., when $\alpha<\phi<\pi$, the vector potential

$$\begin{aligned}&\sum_{m=0}^{\infty}{}'\operatorname{res}\{[F_+^{(e)}(\nu)-F_-^{(e)}(\nu)]\cos\nu\Omega\ \text{at}\ \nu=\nu_m\}\\&\quad=\sum_{n=-\infty}^{\infty}\delta\left[\Omega-\frac{2n-M+N}{M}\pi\right]\\&\qquad\cdot\left\{\frac{\Gamma(M-N)}{2(M^2-\Gamma^2N^2)}+\frac{\Gamma}{2}\sum_{i=1}^{M-1}\frac{\operatorname{sgn}nU_{|n|-1}(y_i)-\operatorname{sgn}(n-M+N)U_{|n-M+N|-1}(y_i)}{MU_{M-1}(y_i)-\Gamma^2NU_{N-1}(y_i)}\right\}\end{aligned} \tag{44}$$

is shown in (52), given at the bottom of the page, with

$$\begin{aligned}\Lambda(\xi,\phi) = {} & \frac{1}{\cosh 2\xi - \cos 2(\Phi-\phi)} \\ & \cdot \left\{ \cosh\left[\left(1+\frac{2}{\pi}\sin^{-1}(\Gamma/2)\right)\xi\right] \right. \\ & \cdot \cos\left[\left(1-\frac{2}{\pi}\sin^{-1}(\Gamma/2)\right)(\Phi-\phi)\right] \\ & - \cosh\left[\left(1-\frac{2}{\pi}\sin^{-1}(\Gamma/2)\right)\xi\right] \\ & \left. \cdot \cos\left[\left(1+\frac{2}{\pi}\sin^{-1}(\Gamma/2)\right)(\Phi-\phi)\right]\right\} \\ & - \frac{1}{\cosh 2\xi + \cos 2(\Phi+\phi)} \\ & \cdot \left\{ \cosh\left[\left(1+\frac{2}{\pi}\sin^{-1}(\Gamma/2)\right)\xi\right] \right. \\ & \cdot \cos\left[\left(1-\frac{2}{\pi}\sin^{-1}(\Gamma/2)\right)(2\pi-\Phi-\phi)\right] \\ & + \cosh\left[\left(1-\frac{2}{\pi}\sin^{-1}(\Gamma/2)\right)\xi\right] \\ & \left. \cdot \cos\left[\left(1+\frac{2}{\pi}\sin^{-1}(\Gamma/2)\right)(2\pi-\Phi-\phi)\right]\right\}. \end{aligned} \tag{53}$$

The spherically spreading delta functions are the geometrical optics field. The argument $\pi - |\Phi - \phi|$ of the first Heaviside step function is always positive in the present case $\alpha = \pi/4 < \phi$, $\Phi < \pi$. That is, the source is directly visible from each field point in this exterior domain. However, the geometrical optics reflection, which is the second term of (52) and is weighted by Γ, disappears beyond the reflection boundary at $\phi = 3\pi/2 - \Phi$, as indicated by its Heaviside factor. Arrival times of these specular contributions are between the extrema T_- and T_+, defined by

$$cT_{\mp} = [(r \mp R)^2 + z^2]^{1/2} \tag{54}$$

in terms of permissible source to observer distances. This restriction is an explicit consequence of the underlying transform analysis of [1]. As indicated in (52), for example, the actual arrival time of each wave event depends on the particular geometry in terms of the angles ϕ, Φ, and α, as well as the nondirectional lengths r, R, and z. The remainder of the field, termed the diffraction, begins when the metric-related variable ξ of (3) becomes operative. This "turn-on" time T_+ corresponds to $\xi = 0$ and is predicted by the generalized Fermat's principle. The physical source of this initial diffraction wave is the apex of the "Keller cone."

When ϕ is measured in the opposite sense to denote a field point on the other side of the symmetry plane, i.e., with the replacement $2\pi - \phi \Rightarrow \phi$, the vector potential is shown in (55), given at the bottom of the next page, with

$$\begin{aligned}\Lambda(\xi,\phi) = {} & \frac{1}{\cosh 2\xi - \cos 2(\Phi+\phi)} \\ & \cdot \left\{ \cosh\left[\left(1+\frac{2}{\pi}\sin^{-1}(\Gamma/2)\right)\xi\right] \right. \\ & \cdot \cos\left[\left(1-\frac{2}{\pi}\sin^{-1}(\Gamma/2)\right)(2\pi-\Phi-\phi)\right] \\ & - \cosh\left[\left(1-\frac{2}{\pi}\sin^{-1}(\Gamma/2)\right)\xi\right] \\ & \left. \cdot \cos\left[\left(1+\frac{2}{\pi}\sin^{-1}(\Gamma/2)\right)(2\pi-\Phi-\phi)\right]\right\} \\ & - \frac{1}{\cosh 2\xi + \cos 2(\Phi-\phi)} \\ & \cdot \left\{ \cosh\left[\left(1+\frac{2}{\pi}\sin^{-1}(\Gamma/2)\right)\xi\right] \right. \\ & \cdot \cos\left[\left(1-\frac{2}{\pi}\sin^{-1}(\Gamma/2)\right)(\Phi-\phi)\right] \\ & + \cosh\left[\left(1-\frac{2}{\pi}\sin^{-1}(\Gamma/2)\right)\xi\right] \\ & \left. \cdot \cos\left[\left(1+\frac{2}{\pi}\sin^{-1}(\Gamma/2)\right)(\Phi-\phi)\right]\right\}. \end{aligned} \tag{56}$$

$$\{\quad\} = \frac{\cosh\left[M\xi - (\xi - i\Psi)\frac{M}{2\pi}\cos^{-1} y_i\right] - (-1)^M \cosh\left[iM\Psi + (\xi - i\Psi)\frac{M}{2\pi}\cos^{-1} y_i\right]}{\cosh M\xi - (-1)^M \cos M\Psi} \tag{49}$$

$$\begin{aligned} A_z^{(e)} = \frac{I\ell}{\epsilon_e} \Bigg\{ & \frac{\delta\left[t - \frac{1}{c}(r^2+R^2+z^2-2rR\cos|\Phi-\phi|)^{1/2}\right]}{4\pi(r^2+R^2+z^2-2rR\cos|\Phi-\phi|)^{1/2}} H(\pi - |\Phi-\phi|) \\ & + \Gamma \frac{\delta\left[t - \frac{1}{c}(r^2+R^2+z^2-2rR\cos(\Phi+\phi-\pi/2))^{1/2}\right]}{4\pi(r^2+R^2+z^2-2rR\cos(\Phi+\phi-\pi/2))^{1/2}} H(3\pi/2 - \Phi - \phi) \\ & - \frac{c\Gamma}{2\pi^2(4-\Gamma^2)^{1/2} rR\sinh\xi}\Lambda(\xi,\phi) \Bigg\} \end{aligned} \tag{52}$$

The third term of (55), which is the ray that penetrates the wedge and emerges on the "shadowed" side, is weighted by the cascaded transmission coefficient $(1-\Gamma)(1+\Gamma)$. Note that this penetration field exists in the shadow region of the source.

The geometrical optics and diffraction parts of the scalar potential are considered separately. Application of (12) to the general form

$$A_z^g = \frac{\delta(t-q/c)}{q}\, H[\pi-(\phi+\beta)]$$

with

$$q^2 = r^2 + R^2 + z^2 - 2rR\cos(\phi+\beta) \tag{57}$$

results in a typical geometrical optics contribution

$$V^g = \frac{z}{q^2}\left[\frac{\delta(t-q/c)}{c} + \frac{H(t-q/c)}{q}\right] H[\pi-(\phi+\beta)] \tag{58}$$

to the scalar potential. The gauge (12) is most conveniently applied to the diffraction field as

$$V^d(r,\phi,\xi) = -\frac{\partial}{\partial z}\int_0^{\xi} A_z^d(r,\phi,\xi')\,\frac{\partial t'}{\partial \xi'}\,d\xi'. \tag{59}$$

Definition (3), the introduction of the arrival time parameter

$$\sigma = \frac{1+(T_-/T_+)^2}{1-(T_-/T_+)^2} > 1 \tag{60}$$

and the pertinent diffraction (last) terms of (52) and (55) permit the representation as shown in (61), given at the bottom of the page. Given the form of (53) and (56), the evaluation of (61) requires integrals of the form

$$\int_0^{\xi} \frac{\cosh a\xi'}{(\cosh 2\xi' + b)(\cosh\xi' + \sigma)^{3/2}}\,d\xi' \tag{62}$$

with parameters $0 < a < 2$, $\sigma > 1$, and $-1 \le b = \mp\cos 2(\Phi \mp \phi) \le 1$. If ϕ lies along one of the geometrical reflection or shadow boundaries, rearrangement of the terms cannot remove the singularity when $b = -1$. Otherwise, the integrand is so well behaved that quadrature is the most efficient method of computation. The following numerical results make use of the IMSL routine QDAGS [14], which treats the nearly singular behavior as $b \to -1$ by a globally adaptive Gauss–Kronrod rule based on the ϵ-algorithm extrapolation.

The Dirac delta functions and Heaviside step functions that comprise the geometrical optics portion of the potentials are clear. The variation of the functions $\Lambda(\xi,\phi)$ and $Q(\xi,\phi;\sigma)$ as a function of ξ for fixed values of ϕ and Φ is graphed in Figs. 2 and 3. The effect of the multiplicative factors $(rR\sinh\xi)^{-1}$ and $z(rR)^{-3/2}$, respectively, in the diffracted components of the vector and scalar potentials is readily apparent without specific numerical values. The two sets of curves in Figs. 2 and 3 use $\Gamma = 0.5$, and for the normalized scalar potential of Fig. 3, the arrival time parameter is $\sigma = 2$. The relative insensitivity of Λ and Q to the values of Γ and σ precludes the need to present an array of parameterized curves and numerical data. The main impact of the dielectric contrast Γ is in the scale factors of the geometrical optics (Fresnel reflection and transmission coefficients) and diffraction components of both potentials. The striking feature of the diffracted potentials of Figs. 2 and 3 is the change in sign across the reflection boundary at $\phi = \pi$, due to the source location at $\Phi = \pi/2$. As the reflection boundary is approached from either side, the initial $(\xi \to 0+)$ diffracted flash becomes stronger and ultimately coincident with the specular reflection. Unlike the full time-harmonic solution, which must be bounded, the direct, reflected, and diffracted waves due to the impulsive current all exhibit singularities that generally arrive at differ-

$$\begin{aligned} A_z^{(e)} = \frac{I\ell}{\epsilon_e}\Bigg\{ & \frac{\delta\left[t-\frac{1}{c}(r^2+R^2+z^2-2rR\cos(2\pi-\Phi-\phi))^{1/2}\right]}{4\pi(r^2+R^2+z^2-2rR\cos(2\pi-\Phi-\phi))^{1/2}}\,H(\phi+\Phi-\pi) \\ & + \Gamma\,\frac{\delta\left[t-\frac{1}{c}(r^2+R^2+z^2-2rR\cos(3\pi/2-|\Phi-\phi|))^{1/2}\right]}{4\pi(r^2+R^2+z^2-2rR\cos(3\pi/2-|\Phi-\phi|))^{1/2}}\,H(|\phi-\phi|-\pi/2) \\ & + (1-\Gamma^2)\,\frac{\delta\left[t-\frac{1}{c}(r^2+R^2+z^2-2rR\cos(\Phi+\phi))^{1/2}\right]}{4\pi(r^2+R^2+z^2-2rR\cos(\Phi+\phi))^{1/2}}\,H(\pi-\Phi-\phi) \\ & - \frac{c\Gamma}{2\pi^2(4-\Gamma^2)^{1/2}rR\sinh\xi}\,\Lambda(\xi,\phi)\Bigg\} \end{aligned} \tag{55}$$

$$V^d(r,\phi,\xi) = \frac{-I\ell\Gamma z}{\epsilon_e\pi^2(4-\Gamma^2)^{1/2}(2rR)^{3/2}}\underbrace{\left[\frac{\Lambda(\xi,\phi)}{\sinh\xi\,(\sigma+\cosh\xi)^{1/2}} + \frac{1}{2}\int_0^{\xi}\frac{\Lambda(\xi',\phi)}{(\sigma+\cosh\xi')^{3/2}}\,d\xi'\right]}_{Q(\xi,\phi;\sigma)} \tag{61}$$

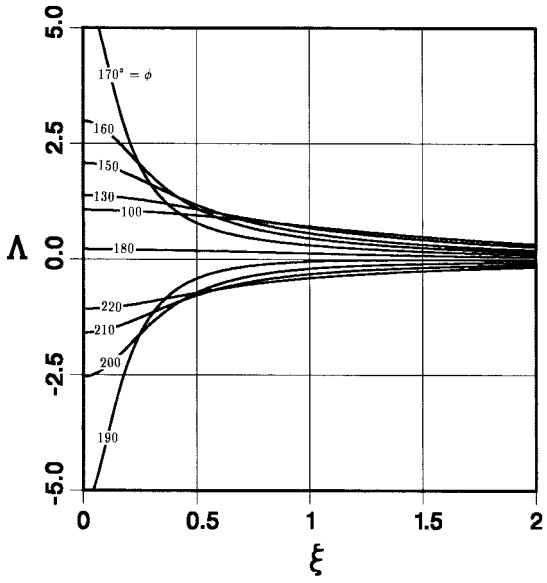

Fig. 2. Scaled diffraction portion of vector potential $\Lambda(\xi, \phi)$ as a function of the metric variable ξ. Case: $\Gamma = 0.5$, $\alpha = \pi/4$, $\Phi = \pi/2$, $100° \leq \phi \leq 220°$.

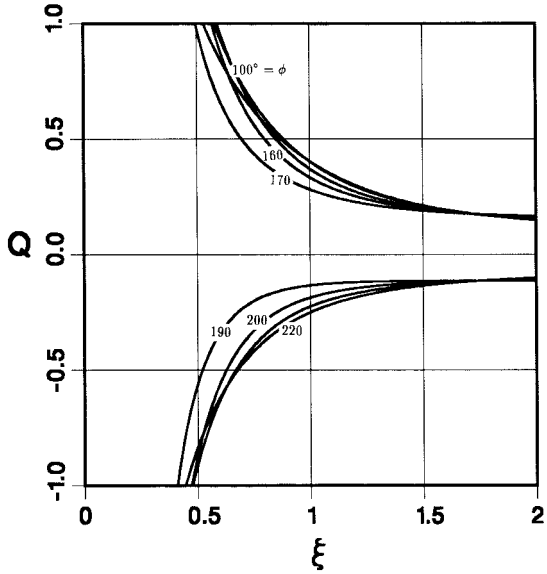

Fig. 3. Scaled diffraction portion of scalar potential $Q(\xi, \phi; \sigma)$ as a function of the metric variable ξ. Case: $\sigma = 2$, $\Gamma = 0.5$, $\alpha = \pi/4$, $\Phi = \pi/2$, $100° \leq \phi \leq 220°$.

ent times. However, the sign of the diffracted singularity is always in opposition to any changes in the geometrical optics singularities. This is especially evident in the neighborhood of the reflection and shadow boundaries, where the various geometrical optics rays are turned on or off.

Long after the impulsive dipole current has been pulsed (at $t = 0$), the variable $\xi \to \infty$ as $t \to \infty$ and the remaining static electric dipole produce the static potential of the second (integral) term of Q in (61). Both the vector potential and the magnetic field have decayed to zero in this static limit. In principle, this asymptotic limit should recover the static results of [15] and [16], with obvious adjustments for the source configuration. However, the present form for the impulsive temporal source hinders a direct comparison [analytic evaluation of $Q(\xi \to \infty)$] with [15] or [16]. With respect to integral transform techniques, the static problem is better treated as such from the outset, as in [15], in terms of the Mellin transform which is the static limit of the Kantorovich–Lebedev transform.

Application of the curl operator of (6) to the geometrical optics terms (57) of the vector potential gives the typical geometrical optics magnetic field

$$\vec{H}^g = \frac{I\ell}{4\pi}\left\{-\hat{r}\left[\frac{R\sin(\phi+\beta)}{q^2} \cdot \left(\frac{\delta(t-q/c)}{q} + \frac{\delta'(t-q/c)}{c}\right)H[\pi-(\phi+\beta)] + \frac{\delta(t-q/c)\delta(\pi-(\phi+\beta))}{rq}\right] + \hat{\phi}\,\frac{r}{q^2}\left(\frac{\delta(t-q/c)}{q} + \frac{\delta'(t-q/c)}{c}\right) \cdot H[\pi-(\phi+\beta)]\right\}. \tag{63}$$

The diffraction contribution to the magnetic field, according to both cases (52) and (55), is

$$\vec{H}^d = \frac{I\ell c\Gamma}{2\pi^2(4-\Gamma^2)^{1/2}}\left\{-\frac{\hat{r}}{r^2 R\sinh\xi}\,\frac{\partial\Lambda(\xi,\phi)}{\partial\phi} + \frac{\hat{\phi}}{rR\sinh^2\xi} \cdot \left[\frac{\Lambda(\xi,\phi)}{\sinh\xi}\left(\frac{1}{r}+\frac{\cosh\xi}{R}\right) - \frac{\partial\Lambda(\xi,\phi)}{\partial\xi}\left(\frac{1}{R}+\frac{\cosh\xi}{r}\right)\right]\right\} \tag{64}$$

in terms of the scalar function Λ of (53) or (56). Similarly, the electric field is given by the second member of (6) in terms of both potentials A_z and V, or equivalently, from the t integration of the curl of $\vec{H}$. Recall that the t integration is introduced into the scalar potential via the auxiliary function Q of (61).

VI. Conclusions

Exact analytic results for the transient electromagnetic fields scattered by the isovelocity wedge are broken into geometrical optics and diffraction contributions. Direct, reflected, and transmitted rays comprise the geometrical optics terms. Under this isorefractivity restriction, the usual Fresnel coefficients are independent of incidence angle. The apparent source of the diffraction field is the wedge apex, with the diffracted rays forming the "Keller cone" in accordance with the generalized Fermat's principle. Scattered electromagnetic fields due to more complicated source configurations can now be synthesized, via appropriate temporal and/or spatial convolutions with the resultant time domain Green's functions.

APPENDIX A
EXAMPLE CALCULATIONS OF GEOMETRICAL OPTICS RESIDUES

Case 1—Wedge Half-Angle $\alpha = \pi/3$: The integers in (24) are now $N = 1$, $M = 3$, and the zeros of

$$1 - \Gamma^2 - T_3(y) + \Gamma^2 y = 0 \implies (1-y)[1 + 4y + 4y^2 - \Gamma^2] = 0 \tag{A.1}$$

are the required values in (38):

$$y_1 = -\tfrac{1}{2}(1+\Gamma) \quad y_2 = -\tfrac{1}{2}(1-\Gamma). \tag{A.2}$$

Consider the coefficient (43)

$$\frac{3-\Gamma^2}{2(9-\Gamma^2)} + \frac{1}{2}\sum_{i=1}^{2} \frac{4y_i^2 - 1 - \Gamma^2}{12y_i^2 - 3 - \Gamma^2} T_{|n|}(y_i) \tag{A.3}$$

in which

$$\frac{4y_i^2 - 1 - \Gamma^2}{12y_i^2 - 3 - \Gamma^2} = \frac{1}{3 \pm \Gamma}$$

and

$$\frac{3-\Gamma^2}{9-\Gamma^2} = \frac{1+\Gamma}{2(3+\Gamma)} + \frac{1-\Gamma}{2(3-\Gamma)} \tag{A.4}$$

so that the required coefficient is

$$\frac{1}{2}\left[\frac{T_n(y_1) - y_1}{3+\Gamma} + \frac{T_n(y_2) - y_2}{3-\Gamma}\right]. \tag{A.5}$$

Evaluation at the values of n that yield delta functions in visible space gives

$$\begin{aligned}
&n = 0 \Rightarrow \tfrac{1}{2}\left[\tfrac{1}{2} + \tfrac{1}{2}\right] = \tfrac{1}{2}\\
&n = 1 \Rightarrow 0\\
&n = 2 \Rightarrow \frac{1}{2}\left[\frac{2y_1^2 - 1 - y_1}{3+\Gamma} + \frac{2y_2^2 - 1 - y_2}{3-\Gamma}\right]\\
&\qquad = \frac{1}{2}\left[\frac{\Gamma^2}{2}\frac{6}{9-\Gamma^2} + \frac{3\Gamma}{2}\frac{-2\Gamma}{9-\Gamma^2}\right] = 0\\
&n = 3 \Rightarrow \frac{1}{2}\left[\frac{4y_1(y_1^2-1)}{3+\Gamma} + \frac{4y_2(y_2^2-1)}{3-\Gamma}\right]\\
&\quad = -y_1(y_1+1) - y_2(y_2+1)\\
&\qquad = \frac{1-\Gamma^2}{2}.
\end{aligned} \tag{A.6}$$

Consider next the coefficient (44)

$$\frac{\Gamma}{9-\Gamma^2} + \frac{\Gamma}{2}\sum_{i=1}^{2} \frac{\operatorname{sgn} n\, U_{|n|-1}(y_i) - \operatorname{sgn}(n-2) U_{|n-2|-1}(y_i)}{12y_i^2 - 3 - \Gamma^2} \tag{A.7}$$

which in view of

$$\frac{\Gamma}{9-\Gamma^2} = -\frac{1}{2}\left(\frac{1}{3+\Gamma} - \frac{1}{3-\Gamma}\right)$$

and

$$\frac{\Gamma}{2(12y_i^2 - 3 - \Gamma^2)} = \frac{\pm 1}{4(3 \pm \Gamma)} \tag{A.8}$$

is written as

$$\frac{1}{4}\left[\frac{\operatorname{sgn} n\, U_{|n|-1}(y_1) - \operatorname{sgn}(n-2) U_{|n-2|-1}(y_1) - 2}{3+\Gamma} - \frac{\operatorname{sgn} n\, U_{|n|-1}(y_2) - \operatorname{sgn}(n-2) U_{|n-2|-1}(y_2) - 2}{3-\Gamma}\right]. \tag{A.9}$$

Explicit values at the pertinent values of n are

$$\begin{aligned}
&n = 0,\ 2 \Rightarrow \frac{1}{4}\left[\frac{2y_1 - 2}{3+\Gamma} - \frac{2y_2 - 2}{3-\Gamma}\right] = \frac{1}{4}[-1\ +1] = 0\\
&n = 1 \Rightarrow 0\\
&n = -1,\ 3 \Rightarrow \frac{1}{4}\left[\frac{U_2(y_1) - 3}{3+\Gamma} - \frac{U_2(y_2) - 3}{3-\Gamma}\right]\\
&\qquad = -\frac{y_1 + 1}{2} + \frac{y_2 + 1}{2} = \frac{\Gamma}{2}.
\end{aligned} \tag{A.10}$$

Case 2—Wedge Half-Angle $\alpha = \pi/4$: With $N = 1$, $M = 2$ the single root from the characteristic equation

$$1 - \Gamma^2 - 2y^2 + 1 + \Gamma^2 y = 0 \implies (1-y)(2 + 2y - \Gamma^2) = 0 \tag{A.11}$$

is

$$y_1 = -1 + \tfrac{1}{2}\Gamma^2. \tag{A.12}$$

Coefficient (43) reduces to

$$\frac{2-\Gamma^2}{2(4-\Gamma^2)} + \frac{1}{2}\frac{2y_1 - \Gamma^2}{4y_1 - \Gamma^2} T_{|n|}(y_1) = \frac{T_{|n|}(y_1) - y_1}{4-\Gamma^2} \tag{A.13}$$

and provides physical delta function weights corresponding to

$$\begin{aligned}
&n = 0 \Rightarrow \frac{1 - y_1}{4-\Gamma^2} = \frac{1}{2}\\
&n = 1 \Rightarrow 0\\
&n = 2 \Rightarrow \frac{2y_1^2 - 1 - y_1}{4-\Gamma^2} = \frac{1-\Gamma^2}{2}.
\end{aligned} \tag{A.14}$$

Coefficient (44) is

$$\frac{\Gamma}{2(4-\Gamma^2)}[1 - \operatorname{sgn} n\, U_{|n|-1}(y_1) + \operatorname{sgn}(n-1) U_{|n-1|-1}(y_1)] \tag{A.15}$$

with contributions

$$\begin{aligned}
&n = 0,\ 1 \Rightarrow \frac{\Gamma}{2(4-\Gamma^2)}(1-1) = 0\\
&n = -1,\ 2 \Rightarrow \frac{\Gamma}{2(4-\Gamma^2)}[1 - 2y_1 + 1] = \frac{\Gamma}{2}.
\end{aligned} \tag{A.16}$$

APPENDIX B
EXAMPLE CALCULATIONS OF DIFFRACTION FIELD RESIDUES

Case 1—Wedge Half-Angle $\alpha = \pi/3$: With $N = 1$, $M = 3$ the two-term sum in (50) or (51) is

$$\begin{aligned}
&\frac{3}{2\pi}\frac{1}{3+\Gamma}\frac{\sin\left[\frac{3}{2}\cos^{-1}\left(-\frac{1+\Gamma}{2}\right)\right]}{\cosh 3\xi + \cos 3\Psi}\\
&\quad \cdot \left\{\cosh\left[\frac{3\xi}{2}\left(1 + \frac{1}{\pi}\cos^{-1}\frac{1+\Gamma}{2}\right)\right]\right.\\
&\qquad \cdot \cos\left[\frac{3\Psi}{2\pi}\cos^{-1}\left(-\frac{1+\Gamma}{2}\right)\right]\\
&\qquad + \cosh\left[\frac{3\xi}{2\pi}\cos^{-1}\left(-\frac{1+\Gamma}{2}\right)\right]\\
&\qquad \left.\cdot \cos\left[\frac{3\Psi}{2}\left(1 + \frac{1}{\pi}\cos^{-1}\frac{1+\Gamma}{2}\right)\right]\right\}\\
&\quad \pm \text{similar expression with } -\Gamma \text{ instead of } \Gamma
\end{aligned} \tag{B.1}$$

where

$$\sin\left[\frac{3}{2}\cos^{-1}\left(-\frac{1+\Gamma}{2}\right)\right]=-\frac{\Gamma}{2}\sqrt{3+\Gamma}. \tag{B.2}$$

Hence, with $\{\quad\}$ denoting the curly brackets in (B.1), the diffraction component of p_s+p_a is $-c/2\pi rR\sinh\xi$ times

$$\begin{aligned}&\frac{3\Gamma}{4\pi\sqrt{3+\Gamma}}\,\frac{1}{\cosh 3\xi+\cos 3(\Phi-\phi)}\Big\{\quad\Big\}_{\Psi=\Phi-\phi}\\&\quad+\text{similar expression with }-\Gamma\text{ instead of }\Gamma\\&\quad+\frac{3\Gamma}{4\pi\sqrt{3+\Gamma}}\,\frac{1}{\cosh 3\xi+\cos 3(\Phi+\phi)}\Big\{\quad\Big\}_{\Psi=2\pi-\Phi-\phi}\\&\quad-\text{similar expression with }-\Gamma\text{ instead of }\Gamma.\end{aligned} \tag{B.3}$$

Case 2—Wedge Half-Angle $\alpha=\pi/4$: With $N=1, M=2$ the single term in (50) is

$$\begin{aligned}&\frac{1}{\pi}\,\frac{2}{4-\Gamma^2}\,\frac{\sin[\cos^{-1}y_1]}{\cosh 2\xi-\cos 2\Psi}\\&\quad\cdot\left\{\cosh\left[\xi\left(1+\frac{1}{\pi}\cos^{-1}(-y_1)\right)\right]\right.\\&\qquad\cdot\cos\left[\Psi\left(1-\frac{1}{\pi}\cos^{-1}(-y_1)\right)\right]\\&\qquad-\cosh\left[\xi\left(1-\frac{1}{\pi}\cos^{-1}(-y_1)\right)\right]\\&\qquad\left.\cdot\cos\left[\Psi\left(1+\frac{1}{\pi}\cos^{-1}(-y_1)\right)\right]\right\}\end{aligned} \tag{B.4}$$

while the single term in (51) is

$$\begin{aligned}&\frac{2\Gamma}{\pi}\,\frac{-\sin\left[\frac{1}{2}\cos^{-1}y_1\right]}{(4-\Gamma^2)[\cosh 2\xi+\cos 2\Psi]}\\&\quad\{\text{as above with }+\text{ instead of }-\}.\end{aligned} \tag{B.5}$$

The simplifications

$$\begin{aligned}\sin\left[\tfrac{1}{2}\cos^{-1}y_1\right]&=\sqrt{1-\Gamma^2/4}\\\sin[\cos^{-1}y_1]&=|\Gamma|\sqrt{1-\Gamma^2/4}\\\cos^{-1}(-y_1)&=2\sin^{-1}(|\Gamma|/2)\end{aligned} \tag{B.6}$$

then enable (53) and (56) to be deduced from (B.4) and (B.5).

REFERENCES

[1] A. M. J. Davis and R. W. Scharstein, "The complete extension of the Biot–Tolstoy solution to the density contrast wedge with sample calculations," *J. Acoust. Soc. Amer.*, vol. 101, no. 4, pp. 1821–1835, Apr. 1997.

[2] M. A. Biot and I. Tolstoy, "Formulation of wave propagation in infinite media by normal coordinates with an application to diffraction," *J. Acoust. Soc. Amer.*, vol. 29, no. 3, pp. 381–391, Mar. 1957.

[3] R. S. Keiffer and J. C. Novarini, "A wedge assemblage method for 3-D acoustic scattering from sea surfaces: Comparison with a Helmholtz–Kirchhoff method," in *Computational Acoustics—Volume 1*, D. Lee, A. Cakmak, and R. Vichnevetsky, Eds. Amsterdam: Elsevier, 1990, pp. 67–81.

[4] L. B. Felsen, "Diffraction of the pulsed field from an arbitrarily oriented electric or magnetic dipole by a perfectly conducting wedge," *SIAM J. Appl. Math.*, vol. 26, no. 2, pp. 306–312, Mar. 1974.

[5] V. A. Borovikov and B. Y. Kinber, *Geometrical Theory of Diffraction.* London, U.K.: IEE, 1994, pp. 352–355.

[6] T. W. Veruttipong, "Time domain version of the uniform GTD," *IEEE Trans. Antennas Propagat.*, vol. 38, pp. 1757–1764, Nov. 1990.

[7] P. R. Rousseau and P. H. Pathak, "Time-domain uniform geometrical theory of diffraction for a curved wedge," *IEEE Trans. Antennas Propagat.*, vol. 43, pp. 1375–1382, Dec. 1995.

[8] L. Knockaert, F. Olyslager, and D. De Zutter, "The diaphanous wedge," *IEEE Trans. Antennas Propagat.*, vol. 45, pp. 1374–1381, Sept. 1997.

[9] P. L. E. Uslenghi, "Exact scattering by isorefractive bodies," *IEEE Trans. Antennas Propagat.*, vol. 45, pp. 1382–1385, Sept. 1997.

[10] E. Marx, "Electromagnetic scattering from a dielectric wedge and the single hypersingular integral equation," *IEEE Trans. Antennas Propagat.*, vol. 41, pp. 1001–1008, Aug. 1993.

[11] A. M. J. Davis, "Two-dimensional acoustical diffraction by a penetrable wedge," *J. Acoust. Soc. Amer.*, vol. 100, pp. 1316–1324, Sept. 1996.

[12] A. D. Rawlins, "Diffraction by a dielectric wedge," *J. Inst. Math Appl.*, vol. 19, pp. 261–279, 1977.

[13] D. S. Jones, *Acoustic and Electromagnetic Waves.* Oxford, U.K.: Clarendon, 1986, p. 462.

[14] IMSL, Inc. *User's Manual: FORTRAN Subroutines for Mathematical Applications*, Houston, TX, 1991, p. 686.

[15] R. W. Scharstein, "Mellin transform solution for the static line-source excitation of a dielectric wedge," *IEEE Trans. Antennas Propagat.*, vol. 41, pp. 1675–1679, Dec. 1993; corrections vol. 42, p. 445, Mar. 1994).

[16] K. I. Nikoskinen and I. V. Lindell, "Image solution for Poisson's equation in wedge geometry," *IEEE Trans. Antennas Propagat.*, vol. 43, pp. 179–187, Feb. 1995.

Robert W. Scharstein, for a photograph and biography, see p. 706 of the May 1994 issue of this TRANSACTIONS.

Anthony M. J. Davis, for a photograph and biography, see p. 706 of the May 1994 issue of this TRANSACTIONS.